1-31-2020

Demarcation of Sepsis-Induced Peripheral and Central Acidosis with pH (Low) Insertion Cycle Peptide

Kelly E. Henry

Aisling M. Chaney

Veronica L. Nagle

Haley C. Cropper

Saghar Mozaffari

See next page for additional authors

Demarcation of Sepsis-Induced Peripheral and Central Acidosis with pH (Low) Insertion Cycle Peptide

Authors

Kelly E. Henry, Aisling M. Chaney, Veronica L. Nagle, Haley C. Cropper, Saghar Mozaffari, Chip Slaybaugh, Keykavous Parang, Oleg A. Andreev, Yana K. Reshetnyak, Michelle L. James, and Jason S. Lewis

Title: Demarcation of Sepsis-Induced Peripheral and Central Acidosis with pH-Low Insertion Cyclic (pHLIC) Peptide

Running title: Demarcating Acidosis with pH-Targeted PET

Authors and Affiliations: Kelly E. Henry,[1] Aisling M. Chaney,[2] Veronica L. Nagle,[1,3,4] Haley C. Cropper,[2] Saghar Mozaffari,[5] Chip Slaybaugh,[6] Keykavous Parang,[5] Oleg A. Andreev,[6] Yana K. Reshetnyak,[6] Michelle L. James,[2,7*] Jason S. Lewis[1,3,4,8*]

[1]Department of Radiology, Memorial Sloan Kettering Cancer Center, New York, NY

[2]Department of Radiology, Stanford University, Stanford, CA

[3]Molecular Pharmacology Program, Memorial Sloan Kettering Cancer Center, New York, NY

[4]Departments of Pharmacology and Radiology, Weill Cornell Medical College, New York, NY

[5]Center for Targeted Drug Delivery, Department of Biomedical and Pharmaceutical Sciences, Chapman University School of Pharmacy, Irvine, CA

[6]Department of Physics, University of Rhode Island, Kingston, RI

[7]Department of Neurology & Neurological Science, Stanford University, Stanford, CA

[8]Radiochemistry and Molecular Imaging Probes Core, Memorial Sloan Kettering Cancer Center, New York, NY

M.L.J. -- mljames@stanford.edu, P: 650-497-0153; F: 650-724-4948 *Co-corresponding author

J.S.L. -- lewisj2@mskcc.org, P: 646-888-3038, F: 646-888-3059, *Co-corresponding author

K.E.H. -- henryk1@mskcc.org, P: 646-888-3271, F: 646-888-3059, Postdoctoral Research Fellow

Financial support: Please refer to acknowledgements section.

ABSTRACT:

Acidosis is a key driver for many diseases, including cancer, sepsis, and neurological disorders. The spatiotemporal dynamics of dysregulated pH across different diseases remains elusive. Moreover, current diagnostic strategies are limited to urine and blood sampling, which do not provide specific localization of pH alterations in the body. We sought to explore if hydrophobic cyclic peptides that partition into the cellular membrane at low extracellular pH (denoted as “pHLIC”) can permit in vivo visualization of acidosis without the selective efficacy required for biomarker-based approaches.

Methods: Acid-sensitive cyclic peptide c[E_4W_5C] pHLIC was conjugated to bifunctional maleimide-NO2A and radiolabeled with copper-64 ($t_{½}$ = 12.7 h). Female C57BL/6J mice were administered an intraperitoneal injection of either LPS (15 mg/kg) or saline (vehicle) and serially imaged with [^{64}Cu]Cu-c[E_4W_5C] (14-15 MBq) over 24 h. Ex vivo digital autoradiography was performed on resected left-hemisphere brain slices and subsequently stained with cresyl violet to enable high-resolution spatial analysis of tracer accumulation. A non- pH-sensitive cell-penetrating control peptide (R_4W_5C) was used to confirm specificity for acidosis in LPS-treated mice. CD11b (macrophage/microglia) and TMEM119 (microglia) immunostaining was performed in brain tissue to correlate levels of neuroinflammation with [^{64}Cu]Cu-c[E_4W_5C] PET signal.

Results: [^{64}Cu]Cu-c[E_4W_5C] radiochemical yield and purity was >95% and >99% respectively, with molar activity >0.925 MBq/nmol. A significant (P < 0.001-0.05) increase in [^{64}Cu]Cu-c[E_4W_5C] uptake was observed in LPS-treated mice (vs. vehicle) within peripheral tissues including blood, lungs, liver, and small intestines. Additionally, there was significantly increased uptake of [^{64}Cu]Cu-c[E_4W_5C] in the brain of LPS-treated

animals. Autoradiographical analysis of brain slices confirmed increased uptake in the cerebellum, cortex, hippocampus, striatum, and hypothalamus of LPS-treated mice (vs. vehicle). This was also reflected in the IHC analysis, which demonstrated a quantitative increase in microglia/macrophage population in the hippocampal region (CD11b), along with qualitative increase in the hypothalamus (CD11b), cortex (both CD11b and TMEM119), and striatum (TMEM119). [^{64}Cu]Cu-c[R_4W_5C] demonstrated significantly reduced uptake in the brain and periphery of LPS mice compared to our acid-mediated [^{64}Cu]Cu-c[E_4W_5C] tracer.

Conclusion: Here, we demonstrate for the first time that a pH-sensitive PET tracer detects acidosis in regions associated with sepsis-driven pro-inflammatory responses. This study suggests that [^{64}Cu]Cu-pHLIC is a valuable tool to noninvasively assess acidosis associated with both central and peripheral innate immune activation.

KEY WORDS: Acidosis, Neuroinflammation, Sepsis, pHLIC, Copper-64

INTRODUCTION

Maintenance of physiological pH is crucial for cellular homeostasis and is closely linked to innate immunological function (*1, 2)*. When an acid-base imbalance occurs with blood and tissue pH becoming acidic – a condition known as acidosis – cellular and immunological dysfunction can occur, resulting in a life-threatening pathogenic state (*3, 4)*. Acidosis is one of the most common diagnoses seen in patients suffering from critical illness such as cardiovascular disease, diabetes, stroke, and sepsis, ultimately resulting in an overabundance of protons in the extracellular medium (*5, 6-10*). These protons can interact with receptors on innate immune cells (e.g. neutrophils, monocytes,

macrophages and NK cells) to drive pro-inflammatory responses (*5, 6)*. Both immune activation and suppression have been reported as a result of acidosis with low pH differentially affecting immune responses depending on cell type and pathways being investigated (*1, 2, 6*).

Acute acidosis lasting from minutes to days is relatively common among critically ill patients (>50%) (*7*), whereas chronic acidosis ranging from weeks to years is less frequent (*8*). In the clinical setting, both acute and chronic acidosis can lead to significant cellular dysfunction in the periphery, along with neuronal damage and aberrant synaptic function centrally (*9*). This pH imbalance has been shown to modulate the immune response and trigger the release of proinflammatory cytokines, which can activate acid-sensing ion channels (ASICs) in the periphery and brain (*3, 10, 11*). Pathologic acidosis and inflammation in peripheral tissues can trigger neuroinflammation and activate microglia in the CNS, implicating an important role for the crosstalk between ASICs and the immune system in neuroinflammatory diseases (*1, 12)*.

Efficient diagnosis and localization of acidosis has potential to greatly impact disease management and patient outcome (*3, 13*). The current method of diagnosing acidosis is via urine sampling (ketoacidosis) and/or arterial blood collection (*4, 14*). Although these methods provide information on the current physiological state, the latter is invasive and neither provides region-specific information regarding the pathologically affected tissues, hence accurate diagnosis and localization can be challenging (*4, 15*). Metabolic acidosis is a common clinical pathology that manifests in different ways affecting a breadth of tissues (*8, 16*), and can acutely affect the CNS (*17*). Since biopsies of the CNS are extremely invasive, there is an unmet need to noninvasively quantify

whole-body acidosis in vivo. Therefore, we sought to develop a probe to specifically detect acidosis with high sensitivity and identify whole-body acid-base alterations, allowing for more informed clinical decisions and disease management.

Previously, we developed a novel class of molecules known as pH (Low) Insertion Peptides (pHLIPs®) that target acidity and utilize a mechanism that does not rely on the selective efficacy of other biomarker technologies (*e.g.* the need for target upregulation at a specific site of disease to delineate from non-target tissues) (*18*). The pHLIP family of peptides target acidity in the cellular microenvironment and have thus far shown utility in tumor imaging and delivery of therapeutic agents (*19-21*). The mechanism of pHLIP entails protonation of negatively-charged residues on a disordered linear peptide sequence in the acidic extracellular microenvironment, resulting in enhancement of peptide hydrophobicity and insertion into phospholipid bilayer of the cell membrane forming a stable transmembrane alpha helix (*18*). This pH-sensitive concept was leveraged to develop a novel class of cyclic peptides (pH (Low) Insertion Cycles, or pHLIC) for enhanced enzymatic stability versus linear peptides (*22*). These cyclic versions consist of negatively charged glutamate residues located at one side of the cycle and hydrophobic tryptophan residues on other (*23*). The glutamate residues are protonated at low extracellular pH to allow for better diffusion of pHLIC into membrane. When equilibrium is established, glutamate residues are de-protonated in cytoplasm preventing pHLIC from exiting the membrane and anchoring cycles into the lipid bilayer.

Since pHLICs have promising properties for blood-brain barrier (BBB) penetration due to their inherent hydrophobic properties and reduced size compared to their linear pHLIP counterparts, we chose to explore a positron emission tomography (PET) labeled

version of a novel pHLIC peptide. We used pHLIC peptides for imaging of peripheral and central acidosis, taking advantage of both the quantitative nature of PET as well as the tracer principle of detecting changes in the acidic microenvironment. We selected the lipopolysaccharide (LPS)-induced mouse model of sepsis, as it is known to exhibit alterations in pH, extensive systemic inflammation, and subtle microglial activation in the brain (*5, 6, 24, 25*).

The aims of this study were to investigate the utility of our novel pH-sensitive radiochemical probe, [^{64}Cu]Cu-c[E_4W_5C] pHLIC, for tracking acidosis in LPS-versus saline-treated mice over the course of 24 h. The central hypothesis of this study was that pH-targeted cyclic peptide probe ([^{64}Cu]Cu-c[E_4W_5C]) will successfully demarcate acidosis through PET and correlate with ex vivo brain uptake and macrophage/microglial activation. In order to confirm our probe's specificity for the acidic microenvironment in this model, we included a [^{64}Cu]Cu-c[R_4W_5C] probe as a negative control. Arginine residues (instead of glutamate in the pH-sensitive peptide) will create a cell-penetrating (*26*), but not via a pH-sensitive mechanism of insertion.

We emphasize that it is not a facile process to take a biopsy of brain tissue. The innovation of this work lies in the ability to noninvasively collect a breadth of information about sepsis-induced acidosis in the whole-body and brain over time using our newly developed PET radiotracer to shed light on the complexities of acidosis.

MATERIALS AND METHODS

Materials. All materials use for synthesis and unless otherwise described, were purchased from Sigma-Aldrich (St. Louis, MO).

Synthesis of pHLIC-NO2A Construct. Peptides were designed and synthesized in the Andreev, Reshetnyak, and Parang labs using solid-phase peptide synthesis techniques. Structures and sequences of all peptides used, including NO2A conjugates and radioconstructs labelled with copper-64 are in Supplemental Fig. 1-4. Cyclic peptide c[E_4W_5C] or c[R_4W_5C] (1 mg, 0.6-0.65 μmol) was mixed with 2× stoichiometric excess NO2A-maleimide (1.2-1.3 μmol) in a 90:10 mixture of anhydrous dimethylformamide (DMF):degassed phosphate-buffered saline (PBS) for 2 h at 37 °C. The conjugate was purified using C_{18} Preparative-HPLC with a 5-95% acetonitrile with 0.1% TFA over 40 min gradient (t_R = 25 min) and evaluated using matrix assisted light desorption-ionization time-of-flight mass spectrometry. Two additional peptides (another cyclic "pHLIC" variant and one linear "pHLIP") were also conjugated to NO2A-maleimide using similar methods. Both pHLIC constructs were chosen for in vivo studies due to their favorable LogP value (Supplemental Table 1) for BBB penetration (*27*). Cyclic peptide c[E_4W_5C] proceeded further due to pilot experiments showing a more favorable BBB penetration, CNS biodistribution, and peripheral detection of acidosis in mice. Doses for animal experiments were diluted in PBS to a maximum concentration of 5% ethanol.

Radiolabeling of pHLIC-NO2A. [^{64}Cu]$CuCl_2$ was obtained from University of Wisconsin Madison (Stanford) and the University of Washington St. Louis (MSK). Each experiment included [^{64}Cu]$CuCl_2$ controls to ensure reproducibility between experiments and institutions. pHLIC-NO2A (20 μL, 16 nmol) was diluted in 0.1 M NH_4Ac (pH 5.5). [^{64}Cu]$CuCl_2$ was added (14-15 MBq) and the reaction proceeded at 80 °C, 800 rpm, for 15 min. [^{64}Cu]Cu-c[E_4W_5C] was purified with a C_{18} Sep Pak with 100% ethanol. Quality control was assessed using instant thin later chromatography using a 50 mM EDTA (pH

5) eluent. Partition coefficient experiments proceeded in a PBS:octanol mixture using previously reported techniques (*28*). Cold labeling of pHLIC-NO2A along with a description of the biophysical measurements of [^{nat}Cu]Cu-c[E_4W_5C] and [^{nat}Cu]Cu-c[R_4W_5C] can be found in the Supplementary Materials.

Animal models. All animal experiments were performed in accordance with the Stanford Administrative Panel on Laboratory Animal Care (APLAC), which is accredited by the Association for the Assessment and Accreditation of Laboratory Animal Care (AAALAC International) or the Institutional Animal Care and Use Committee at Memorial Sloan Kettering Cancer Center. Female C57BL/6J were ordered from Jackson Laboratories at 6-8 weeks of age. LPS from *Escherichia coli* was ordered from Sigma-Aldrich and prepared in sterile saline at a concentration of 3 mg/kg. LPS was injected intraperitoneally (i.p.) 3 h prior to [^{64}Cu]Cu-c[E_4W_5C] administration (15 mg/kg), and saline was used as a vehicle control.

Biodistribution studies. Ex vivo gamma counting was performed to measure the uptake of the radioconjugate in tissues at 12 and 24 h post-radiotracer administration. Blood was collected via cardiac puncture prior to PBS perfusion. Brain and other tissues were harvested and weighed wet. The radioactivity within each organ was counted using a Hidex Automatic γ-counter. Tracer uptake expressed as percentage injected dose per gram (% ID/g) was calculated as the radioactivity associated with each tissue divided by the organ mass and the decay-corrected injected dose at the time of counting, as determined by a calibration curve established via serial dilution of the ^{64}Cu-labelled peptide.

PET/CT Imaging. Radiotracer (16-20 nmol, 14-15 MBq in sterile PBS, 130-150 μL) was injected intravenously and CT and 10 min static PET images were acquired at 1, 5, 9, and 20 h post-injection of radiotracer (4, 8, 12, and 24 h post-LPS inoculation) using a dual microPET/CT scanner (Inveon, Siemens). PET imaging time points with [^{64}Cu]Cu-pHLIC were adapted from a time course previously established by Demoin et al. (*20*). Brain PET quantitation was done using VivoQuant software (version 3.0, InviCRO) in accordance with procedures described by Chaney et al. (*29*).

Autoradiography and Nissl staining. Ex vivo autoradiography was performed according to previously described methods (*30*) using 40 μm-thick left-hemisphere coronal brain sections collected at 12 and 24 h post-injection of [^{64}Cu]Cu-c[E_4W_5C]. Anatomy of brain sections was confirmed by Nissl staining (cresyl violet acetate), using standard techniques. After exposing tissues to digital autoradiography films for 10 half-lives, each film was scanned using a Typhoon phosphorimager. ImageJ software version 2.0.0 was used to visualize images.

Immunohistochemistry. For semiquantitative evaluation of activated microglia and inflammation, staining of CD11b and TMEM119 was performed on 5 μm coronal brain sections, respectively, using previously described methods (*30, 31*).

Statistical Considerations. GraphPad Prism (version 7; GraphPad Software) was used for statistical analyses of the data. Biodistribution data were analyzed by the unpaired, two-tailed Student's *t*-test and differences at the 95% confidence level. All other data were analyzed via 1-way or 2-way ANOVAs with multiple comparisons. P values of 0.05 or less were considered significant.

RESULTS

Synthesis and Radiolabeling of pHLIC. Peptide-chelator conjugates c[E_4W_5C]-NO2A and c[R_4W_5C]-NO2A were produced in 55-60% yield with >99% purity. Further characterization was done using matrix-assisted light desorption time-of-flight (MALDI-ToF) and/or liquid chromatography mass spectrometry (LCMS). MALDI-ToF results: c[E_4W_5C]-NO2A $[M+H]^+$ = m/z: 1977.21 *m/z*; c[R_4W_5C]-NO2A $[M+H]^+$ = m/z: 2085.11 *m/z*. LCMS results: [^{nat}Cu]Cu-c[E_4W_5C] $[M+5H]^+$ = m/z: 428.2 *m/z*; [^{nat}Cu]Cu-c[R_4W_5C] $[M+5H]^+$ = 446.7 m/z: *m/z*. Radiochemical yield and molar activity for all pHLIC conjugates were >95% and >0.925 MBq/nmol respectively. Radiochemical purity was >99% for all peptide conjugates (Supplemental Fig. 4), and [^{64}Cu]Cu-c[E_4W_5C] was >90% stable in serum out to 48 h (Supplemental Fig. 5). Measured Log P values of [^{64}Cu]Cu-c[E_4W_5C] were found to be 2.5 $\pm$ 0.6 at pH 6 and 2.0 $\pm$ 0.2 at pH 7.4 (*n* = 5 replicates per run; 3 independent measurements) (Supplemental Table 1).

In Vivo Study Design. Mice were administered 15 mg/kg LPS i.p to induce sepsis. The onset of acidosis has been reported to manifest peripherally as early as 4 h post-LPS injection, hence we chose this as our first time point to study the pharmacokinetics of our radiotracer (25). Microglial activation occurs within 24 h post-LPS administration in mice (*12, 32*). In order to study alterations in acidosis-induced inflammation in vivo over time, [^{64}Cu]Cu-c[E_4W_5C] was injected 3 h post-LPS induction and serial static PET images were acquired at 1, 5, 9, and 21 h post-radiotracer injection (corresponding to 4, 8, 12, and 24 h post-LPS induction). Fig. 1 illustrates this workflow along with the mechanism of pHLIC peptides' interaction with membrane during acidotic conditions.

PET and Ex Vivo Biodistribution. Serial PET images acquired over the course of 24 h show a clear difference in peripheral [^{64}Cu]Cu-c[E_4W_5C] uptake in vehicle vs. LPS-treated mice (Fig. 2) in tissues affected by acidosis. Supplemental Figs. 17 and 18 represents pilot data for [^{64}Cu]Cu-[E_5K]W_5C PET, biodistribution, and dynamic PET. Less uptake and brain specificity was observed with [^{64}Cu]Cu-[E_5K]W_5C vs. [^{64}Cu]Cu-NO2A-c[E_4W_5C] PET, hence the rationale for moving forward with [^{64}Cu]Cu-NO2A-c[E_4W_5C] for all subsequent studies. CT-guided quantitation of PET images demonstrated statistically significant increases in [^{64}Cu]Cu-c[E_4W_5C] uptake in the kidneys, liver, lungs, and small intestine of LPS mice over 24 h (Fig. 2). Each of these selected tissues demonstrated significantly higher uptake of radiotracer in LPS mice at all time points except in kidneys at 4 h post-LPS injection. Full ex vivo biodistribution (for 12 and 24 h time points) is reported in Supplemental Table 2 and supports the in vivo findings (n = 4/group). PET quantitation of selected regions is represented in Supplemental Table 3 (n = 4/group). Zoomed in rescaled images show uptake of [^{64}Cu]Cu-c[E_4W_5C] in the brain are represented in Fig. 3 for 12 and 24 h time points. Full brain atlas quantification, along with additional brain PET images at 4 and 8 h, including views in the frontal cortex and cerebellum for 12 and 24 h, can be found in Supplemental Figs. 7-10. Supplemental Fig. 19 represents the brain atlas legend for the inVICRO PET quantification. A repeat cohort of [^{64}Cu]Cu-c[E_4W_5C] was done in tandem with negative control tracer [^{64}Cu]Cu-c[R_4W_5C] to highlight specificity of our pHLIC radtioracer for acidosis (Fig. 7). Full ex vivo quantification for these studies (brain and periphery) studies can be found in Supplemental Figs. 11-15 and Supplemental Tables 6-8.

A statistically significant (P < 0.001-0.05) increase in [^{64}Cu]Cu-c[E_4W_5C] uptake was observed in the brain of LPS-treated mice (vs. vehicle) in several regions, many of which have been reported to exhibit inflammation (cerebellum, cortex, hippocampus, hypothalamus, striatum, and midbrain) in this model (Fig. 3) (12, 33-36). Full PET quantitation (of all brain regions) can be found in Supplemental Table 4 for all time points.

Autoradiography. Autoradiographical analysis of brain slices qualitatively confirmed increased uptake of the radiotracer in the cerebellum, cortex, hippocampus, and hypothalamus of LPS-treated mice (vs. vehicle) (Fig. 4). Many of these regions have been identified as key regions affected by neuroinflammation (12, 33). Marked signal was also observed in the choroid plexus and ventricles of both vehicle and LPS-treated mice. We repeated this cohort with to show a significant uptake of [^{64}Cu]Cu-c[E_4W_5C] vs. negative control peptide [^{64}Cu]Cu-c[R_4W_5C] in a number of key regions (Fig. 6).

Immunohistochemistry. Immunohistochemical staining of CD11b and TMEM119 24 h post-LPS treatment show an increase in macrophage/microglia infiltration in the brain. A significant increase in number of CD11b$^+$ cells (coupled with a more ameboid-like in morphology) in the hippocampal region of the brain was observed in LPS-treated mice compared to vehicle (Fig. 5). A qualitative increase of macrophage/microglia is also observed in the hypothalamus and cortex. A subtle increase in TMEM119 represents increased innate immune infiltration that is specific to microglia (36, 37) in the cortex and striatum (Supplemental Fig. 16). This data aligns with previous reports demonstrating increased neuroinflammation in the LPS model correlating to innate immune activation (5, 38, 39) and also mirrors the increased uptake of [^{64}Cu]Cu-c[E_4W_5C] observed via PET and autoradiography in LPS-treated mice.

DISCUSSION

We report the first investigation of a pH-sensitive PET tracer for tracking acidosis in a murine model of sepsis. We have shown the potential of this tool to shed light on the connection between acidosis and innate immune activation over the course of 24 h during the onset of sepsis. Such a radiotracer could enable disease tracking not only in sepsis but in other disorders that exhibit clinical acidosis, including diabetes and stroke. Many groups are working to assess neuroinflammation noninvasively with PET, and the latest in this field is thoroughly reviewed by Narayanaswami et al. (*40*). Our study aims to identify acid-base imbalances in the periphery and the brain by targeting the acidic microenvironment, a specific danger signal in sepsis, and strengthen the connection between acidosis and neuroinflammation.

Acidosis can be a life-threatening condition and is currently poorly understood with regard to whole-body progression, specific regional involvement, and interventions (*4, 8*). One approach being explored to assess the spatiotemporal dynamics of acidosis is Chemical Exchange Saturation Transfer (CEST) magnetic resonance imaging (MRI), and is well-described by Pagel and coworkers (*41, 42*). CEST-MRI exploits a specific MR frequency to generate an image while combining the specificity of magnetic resonance spectroscopy (MRS) with the spatial resolution of MRI (*43*). Recently, CEST-MRI is being investigated to improve analyses of tumor metabolism in the context of acidosis. Additionally, Longo and coworkers have combined CEST-MRI and [^{18}F]FDG to explore the relationship between acidosis and hyperglycolysis within the tumor microenvironment (44) and found that there is a correlation between low extracellular pH and glucose uptake. We have observed a similar correlation with various pHLIP variants (unpublished

data). Additionally, several groups have paved the way for hyperpolarized MR for imaging metabolic acidosis, including for neuroinflammatory disorders (*45, 46*). However, hyperpolarized MR presents technical challenges for clinical translation due to its rapid decay in signal. Our pH-sensitive PET agent utilizes a single dose to assess acidosis and obtain dynamic information of a system in constant flux with ultra-high sensitivity.

The most attractive application of pHLIP and pHLIC imaging platforms is the ability to target highly dynamic changes in the acidic microenvironment without needing to wait for slower changes in expression of a specific receptor. Relying on a probe to target a protein of interest can pose difficulties for clinical translation, especially when BBB penetration is desired (*47*). The design of our radiotracer includes a single point of conjugation, which does not affect the properties of its pH-targeting capabilities (*23*), which is futher evidenced by our biophysical measurements (Supplemental Fig. 6). Once acidosis has gone beyond peripheral damage to affect the CNS, it poses a much more challenging clinical situation (*17*), hence early and spatiotemporal detection is critical. Among the tested pHLIPs and pHLICs, c[E_4W_5C] showed the best BBB penetration and the highest sensitivity for detecting disease-associated alterations in pH, and was therefore selected for detailed investigation. In this study, we were able to exploit the sensitive, quantitative, and longitudinal characteristics of PET imaging to understand both the spatial and temporal dynamics of acidosis.

The molecular mechanisms of how pH imbalance leads to cell damage are both diverse and complicated. Adversarial pH changes outside physiological norm can affect a number of biochemical systems, including cell development and degradation, energy metabolism, and neuronal function (e.g. metabolism of transmitter constituents) (*8*). There

have been studies that report the consequences of metabolic acidosis and how it affects tissues such as the liver, kidneys, and intestines (*8, 53*). ASICs are activated in the presence of inflammation, further perpetuating adverse immune responses, which can lead to significant neuroinflammation over the course of 24 h (*12, 39*). The utility of our pHLIC probe to not only detect systemic but also CNS inflammation makes this approach attractive for investigating pH alterations in a vast number of applications, including stroke and multiple sclerosis. These neurodegenerative diseases involve complex immune and acidotic processes in the brain and peripheral tissues (e.g. spleen, lymph nodes, intestines). The peripheral uptake of pHLIC in regions associated with acidosis in the LPS mouse model (e.g. lung, liver, kidneys, and small intestine) could be predictive of neuroinflammation and activation of microglia in the brain, which we observe as early as 12 h. There are a number of novel therapeutics in the works that aim to treat metabolic acidosis and seek to target acid-sensing ion channels (*48-52*). We posit that our radiotracer would serve as a successful readout for these types of therapies to improve clinical outcomes of acidosis.

CONCLUSION

[^{64}Cu]Cu-c[E_4W_5C] pHLIC is a valuable tool to noninvasively and longitudinally demarcate the spatiotemporal evolution of acidosis in LPS-induced sepsis. We believe that [^{64}Cu]Cu-c[E_4W_5C] has potential applications for other diseases tied to neuroinflammation and is currently being investigated. We expect that our pHLIC radiotracer will serve to increase understanding of the complex relationship between acidosis, immune function, and inflammation.

DISCLOSURES

J.S.L., O.A.A., and Y.K.R. are founders of pHLIP, Inc. They have shares in the company, but the company did not fund any part of the work reported in the paper, which was done in their academic laboratories. No other potential conflicts of interest (financial or otherwise) relevant to this article exist.

ACKNOWLEDGEMENTS

We gratefully acknowledge the Small Animal Imaging Core at MSK and Stanford University. The Radiochemistry and Molecular Imaging Probe core (MSK) was supported in part by NIH grant P30 CA08748. K.E.H. would like to acknowledge the Center for Molecular Imaging and Nanotechnology (CMINT) Tow Fellowship through MSK. M.L.J. would like to acknowledge gift funds for the completion of much of this work in her academic laboratory. We would like to acknowledge the financial support from NIH R01 GM073857-09A1 grant to Y.K.R. and O.A.A for pHLIP technologies. S.M and K.P. would like to acknowledge the Chapman University School of Pharmacy for their core facility and S.M.'s Ph.D. fellowship.

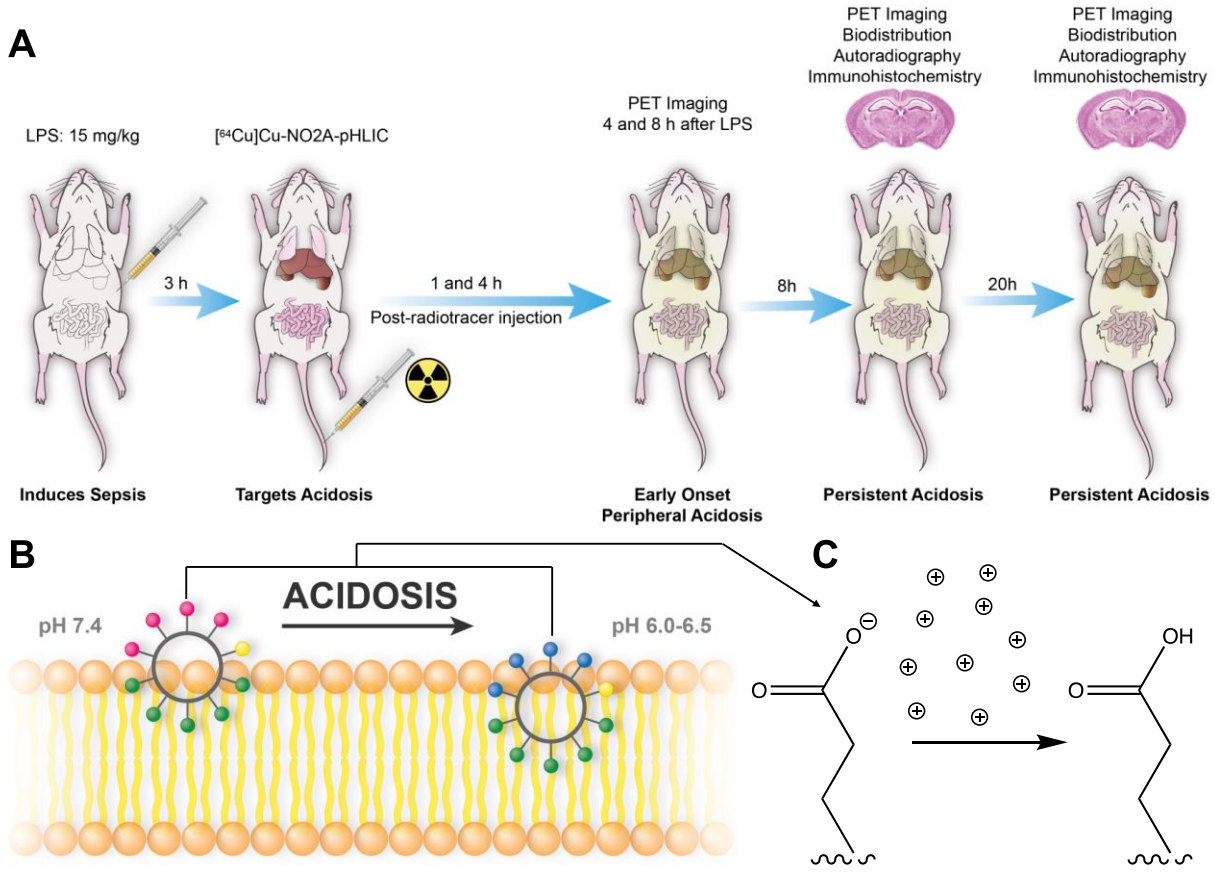

FIGURE 1. Schematic depicting general workflow to tracking acidosis and mechanism of membrane insertion. (A) LPS was injected i.p. into C57BL/6J mice and ^{64}Cu-labelled pHLIC radiotracer was injected 3 h later. Mice underwent PET imaging at 4, 8, 12, and 24 h post-LPS treatment. Autoradiography and immunohistochemistry were performed at 12 and 24 h post-LPS treatment. (B) Mechanism of cyclic peptide insertion into the cellular membrane. pHLICs consist of negatively charged glutamate residues located at one side of the cycle and hydrophobic tryptophan residues on other side of the cycle. The glutamate residues are protonated at low extracellular pH to allow for better diffusion of pHLIC into membrane. When equilibrium is established, glutamate residues are de-protonated in cytoplasm preventing pHLIC to exit out from the membrane and anchoring

cycles into the lipid bilayer. Pink circles represent glutamate residues, which become blue upon protonation as they insert into the membrane. Green circles represent tryptophan residues, and yellow circle is the cysteine residue, which is the point of conjugation the NO2A chelator to enable ^{64}Cu-labeling. (C) Example protonation of glutamate residues in the acidic microenvironment.

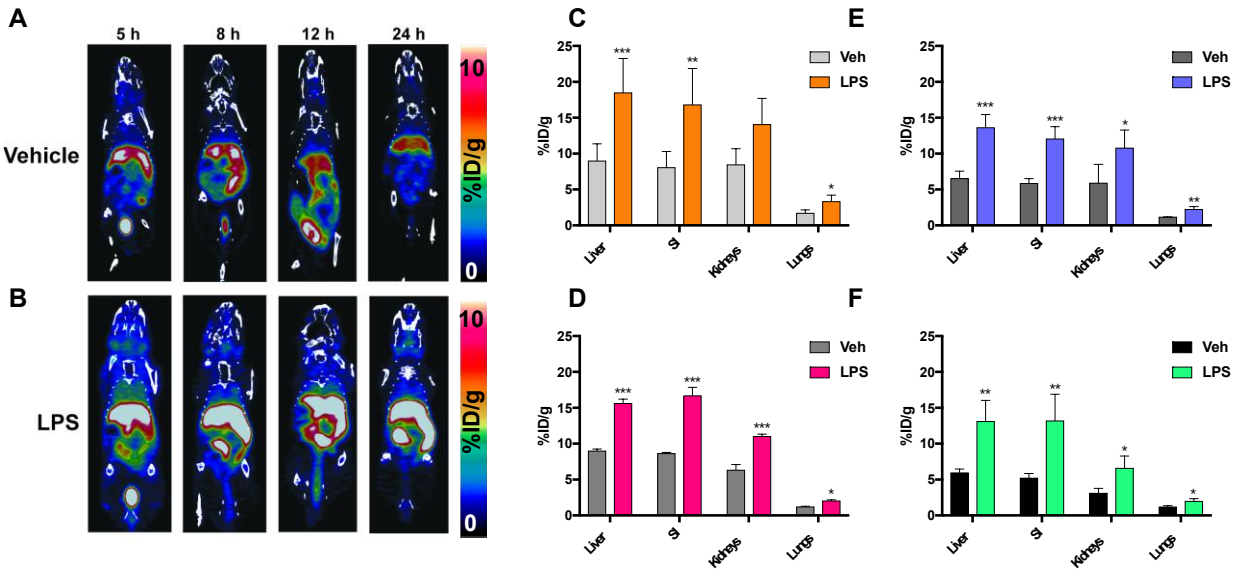

FIGURE 2. [^{64}Cu]Cu-c[E$_4$W$_5$C] pHLIC detects the presence and persistence of acidosis via serial PET imaging over the course of 24 h. (A) PET images of vehicle-treated animals vs. (B) LPS-treated mice at 4, 8, 12, and 24 h post-LPS injection. Peripheral quantitation of PET organs was performed by manually drawing regions of interest around select tissues at 4 h (C), 8 h (D), 12 h (E), and 24 h (F), post-LPS inoculation. Data is represented as average %ID/g ± SD with *n* = 4 animals/group.

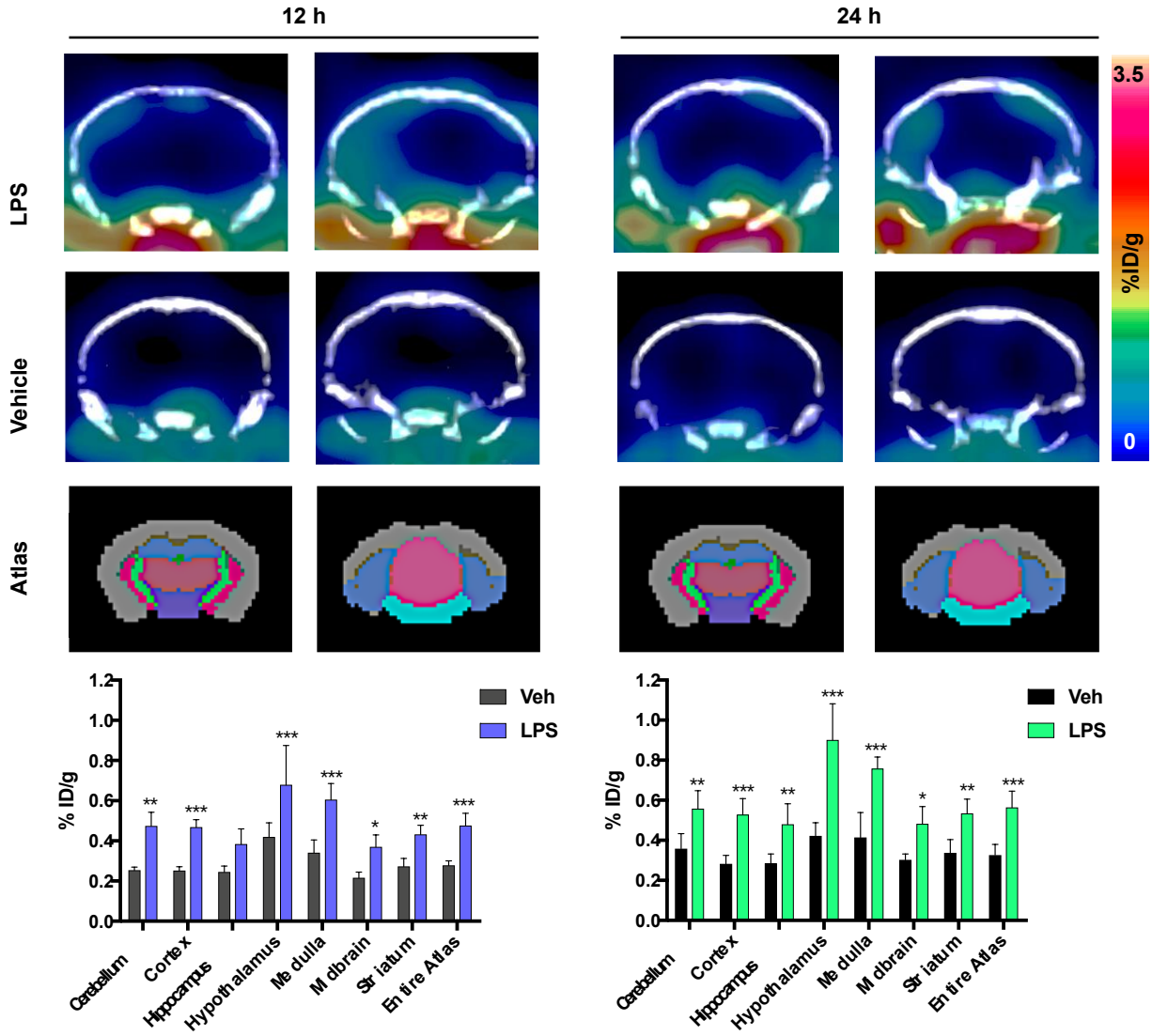

FIGURE 3. [^{64}Cu]Cu-c[E$_4$W$_5$C] pHLIC detects the presence and persistence of acidosis in the brain via PET imaging and 12 and 24 h. Coronal brain slices of [^{64}Cu]Cu-c[E$_4$W$_5$C] PET and brain-atlas guided PET quantitation of vehicle vs. LPS-treated mice is represented. PET imaging of LPS-treated mice at 12 and 24 h are displayed side-by-side with vehicle-treated mouse brains, with corresponding brain atlas to indicate region. Respective quantitation of brain regions was achieved using VivoQuant and is shown at 12 h (left) and 24 h (right). Data is represented as average %ID/g ± SD with *n* = 4 animals/group.

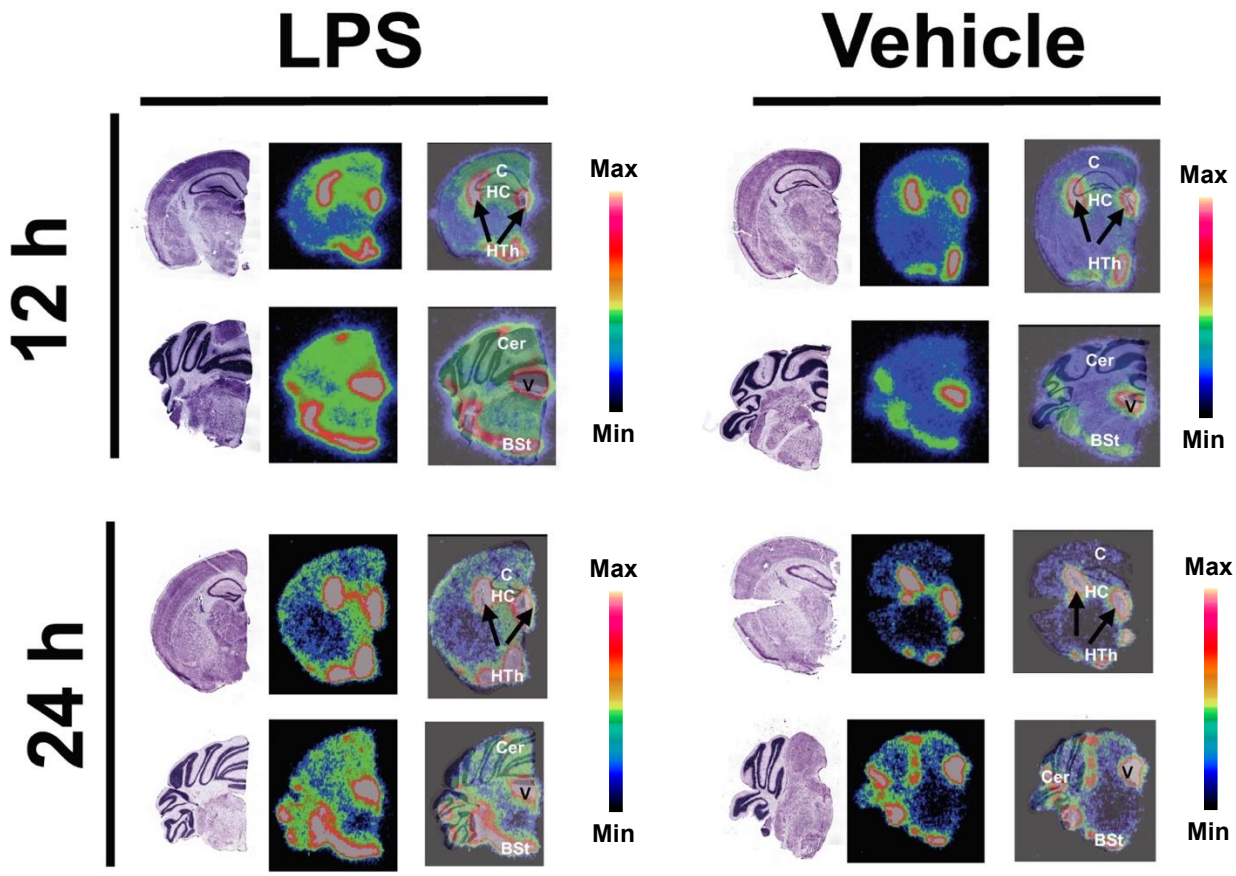

FIGURE 4. Autoradiography enables high-resolution [^{64}Cu]Cu-c[E_4W_5C] pHLIC uptake in left-hemisphere brain slices. Brain slices exposed for autoradiography were stained with cresyl violet to correlate with Nissl bodies to highlight respective anatomy. Abbreviations on autoradiography/Nissl overlay: Cer: cerebellum; C: Cortex; HC: Hippocampus; Hth: Hypothalamus; BSt: brain stem; V: ventricle. Data is represented as average %ID/g ± SD with *n* = 3 animals/group.

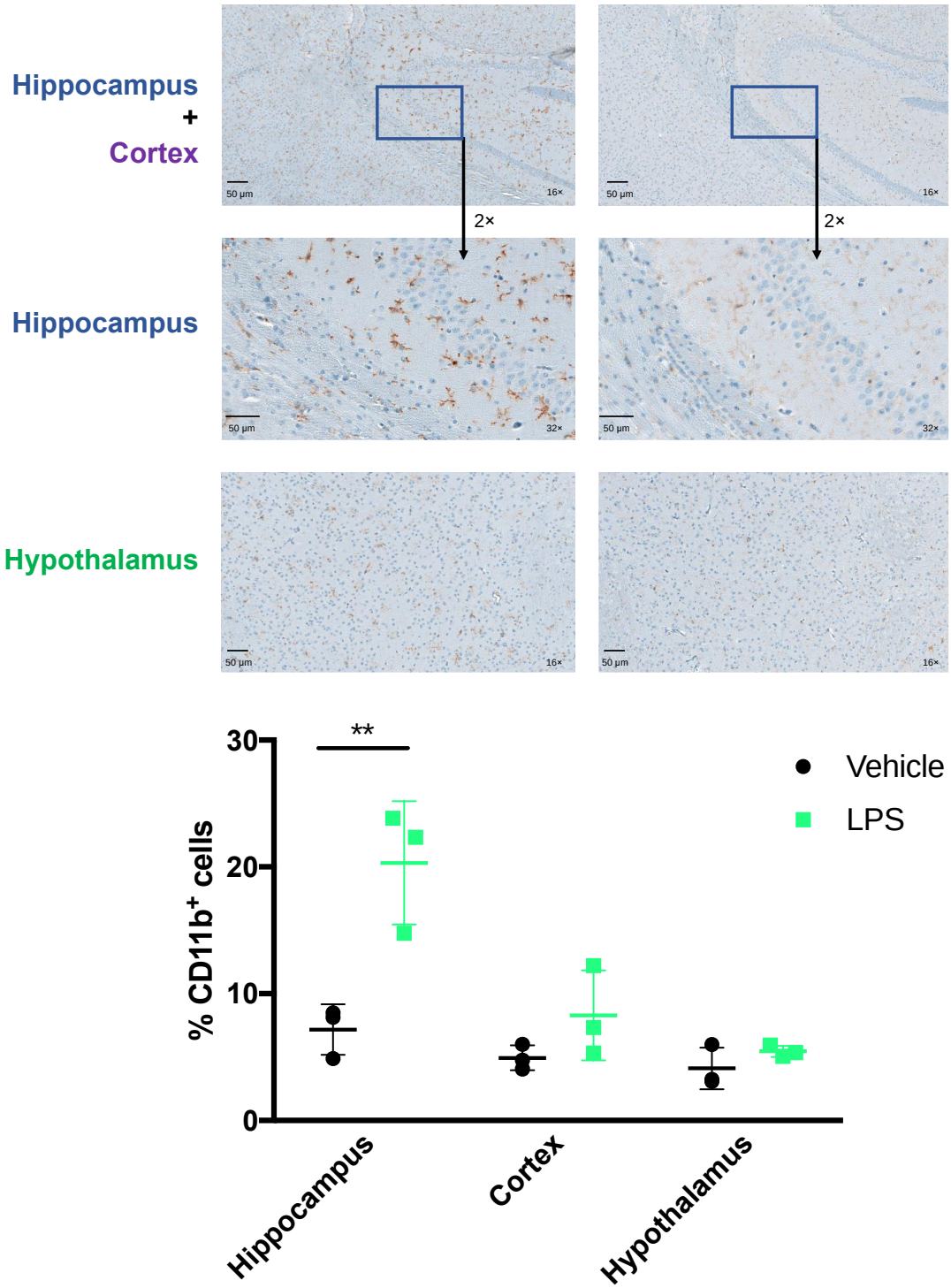

FIGURE 5. Immunohistochemical analysis of CD11b staining identifies an increase of microglia/macrophages in select brain regions of LPS-treated compared to vehicle-treated mice. Data is represented as average %ID/g ± SD with *n* = 3 animals/group.

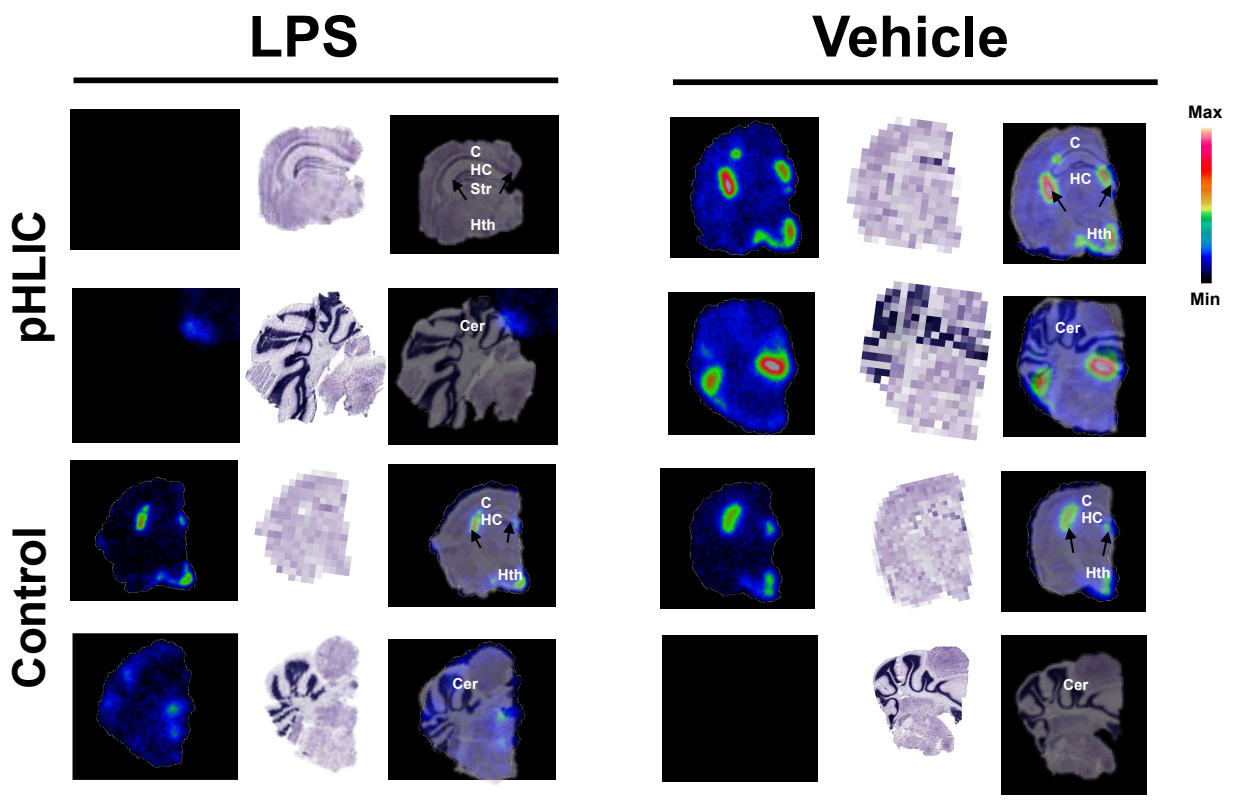

FIGURE 6. Autoradiography enables high-resolution [^{64}Cu]Cu-c[E_4W_5C] pHLIC (top) vs. [^{64}Cu]Cu-c[R_4W_5C] control (bottom) uptake in right-hemisphere brain slices 24 h post-LPS administration. Brain slices exposed for autoradiography were stained with cresyl violet to correlate with Nissl bodies to highlight respective anatomy. Abbreviations on autoradiography/Nissl overlay: Cer: cerebellum; C: Cortex; HC: Hippocampus; Hth: Hypothalamus; Str: striatum. Data is represented *n* = 3 animals/group (vehicle) and *n* = 2 animals/group (LPS).

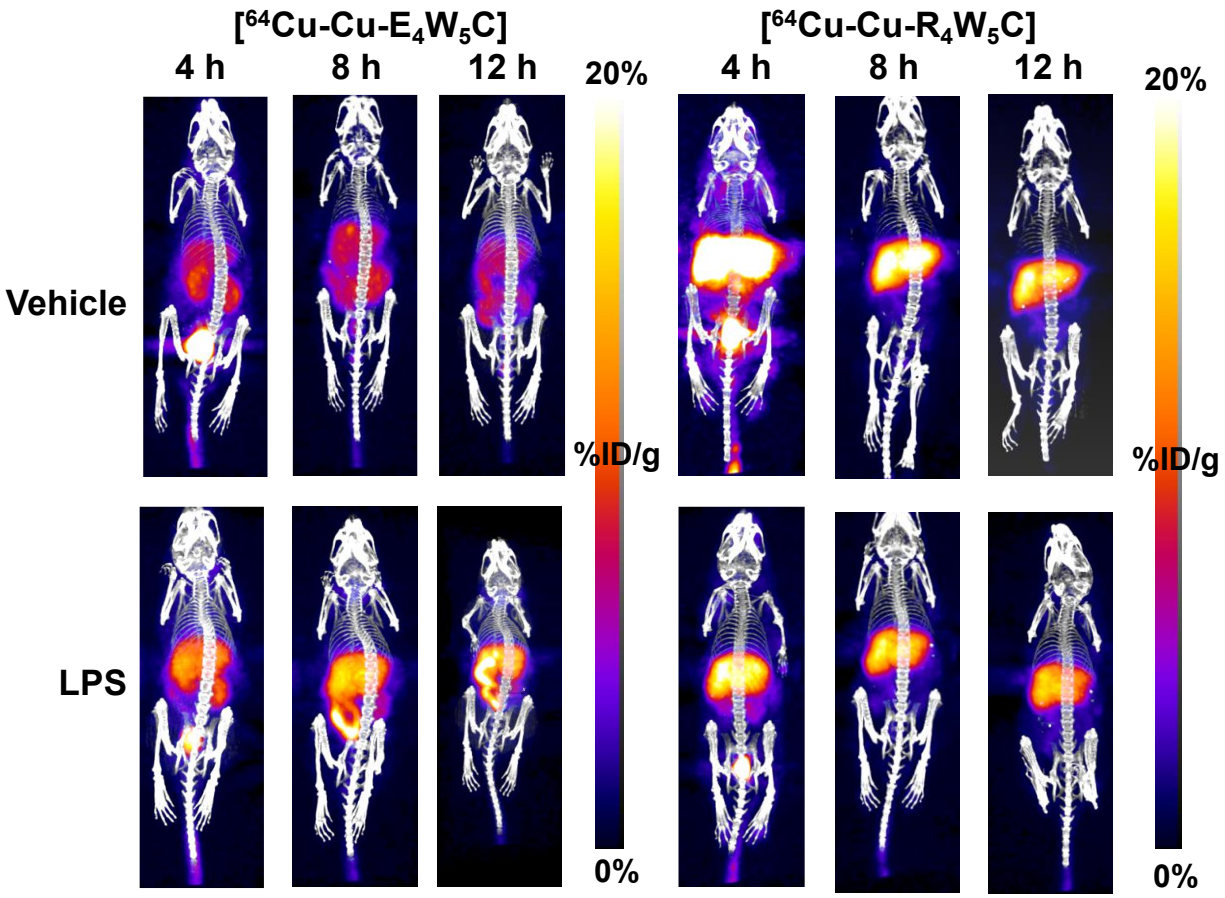

FIGURE 7. Serial PET imaging of [^{64}Cu]Cu-c[E_4W_5C] vs. [^{64}Cu]Cu-c[R_4W_5C] (control) highlights the specificity of pHLIC for acidosis in LPS-induced acidosis over the course of 12 h. Maximum intensity projections of [^{64}Cu]Cu-c[R_4W_5C] show mainly clearance of the radiotracer with no difference between vehicle and LPS-treated mice. Maximum intensity projections of [^{64}Cu]Cu-c[E_4W_5C] uptake represents small intestine, spleen, and kidneys, with a clear difference noted between vehicle and LPS-treated mice. Representative images selected from a pool of *n* = 4 animals/group. PET quantitation of peripheral tissues and brain signal can be found in the supplemental information.

KEY POINTS

QUESTION: The *central hypothesis* of this study is that our pH low-insertion cyclic (pHLIC) peptide probe ([^{64}Cu]Cu-c[E_4W_5C]) will successfully demarcate acidosis in a mouse model of sepsis in a manner that correlates with ex vivo brain uptake and microglial activation.

PERTINENT FINDINGS: We demonstrate for the first time that a pH-sensitive PET tracer detects acidosis in regions associated with sepsis-driven pro-inflammatory responses. We observed significantly increased ($P < 0.05$) uptake of [^{64}Cu]Cu-c[E_4W_5C] in the periphery and brain, which is mirrored by an increase in macrophage/microglial activation in these same regions.

IMPLICATIONS FOR PATIENT CARE: Our study suggests that [^{64}Cu]Cu-pHLIC is a valuable tool to noninvasively assess acidosis associated with both central and peripheral innate immune activation, and has potential to increase understanding of the dynamic relationship between acidosis and inflammation.

REFERENCES

1. Riemann A, Wußling H, Loppnow H, Fu H, Reime S, Thews O. Acidosis differently modulates the inflammatory program in monocytes and macrophages. Biochimica et Biophysica Acta (BBA) - Molecular Basis of Disease. 2016;1862(1):72-81. doi: https://doi.org/10.1016/j.bbadis.2015.10.017.

2. D E, #x00ED, az F, Dantas E, Geffner J. Unravelling the Interplay between Extracellular Acidosis and Immune Cells. Mediators of Inflammation. 2018;2018:11. doi: 10.1155/2018/1218297.

3. Casimir GJ, Lefèvre N, Corazza F, Duchateau J, Chamekh M. The Acid-Base Balance and Gender in Inflammation: A Mini-Review. Front Immunol. 2018;9:475-. doi: 10.3389/fimmu.2018.00475. PubMed PMID: 29593728.

4. Wiederseiner J-M, Muser J, Lutz T, Hulter HN, Krapf R. Acute Metabolic Acidosis: Characterization and Diagnosis of the Disorder and the Plasma Potassium Response. Journal of the American Society of Nephrology. 2004;15(6):1589-96. doi: 10.1097/01.Asn.0000125677.06809.37.

5. Tyrtyshnaia AA, Lysenko LV, Madamba F, Manzhulo IV, Khotimchenko MY, Kleschevnikov AM. Acute neuroinflammation provokes intracellular acidification in mouse hippocampus. Journal of Neuroinflammation. 2016;13:283. doi: 10.1186/s12974-016-0747-8. PubMed PMID: PMC5094044.

6. Rajamäki K, Nordström T, Nurmi K, Åkerman KEO, Kovanen PT, Öörni K, Eklund KK. Extracellular acidosis is a novel danger signal alerting innate immunity via the NLRP3 inflammasome. The Journal of biological chemistry. 2013;288(19):13410-9. Epub 2013/03/25. doi: 10.1074/jbc.M112.426254. PubMed PMID: 23530046.

7. Gunnerson KJ, Saul M, He S, Kellum JA. Lactate versus non-lactate metabolic acidosis: a retrospective outcome evaluation of critically ill patients. Critical care (London, England). 2006;10(1):R22-R. Epub 2006/02/10. doi: 10.1186/cc3987. PubMed PMID: 16507145.

8. Kraut JA, Madias NE. Metabolic acidosis: pathophysiology, diagnosis and management. Nature Reviews Nephrology. 2010;6:274. doi: 10.1038/nrneph.2010.33.

9. Wang Y-C, Li W-Z, Wu Y, Yin Y-Y, Dong L-Y, Chen Z-W, Wu W-N. Acid-sensing ion channel 1a contributes to the effect of extracellular acidosis on NLRP1 inflammasome

activation in cortical neurons. Journal of Neuroinflammation. 2015;12(1):246. doi: 10.1186/s12974-015-0465-7.

10. Bilbo SD, Schwarz JM. The immune system and developmental programming of brain and behavior. Frontiers in neuroendocrinology. 2012;33(3):267-86. Epub 2012/09/09. doi: 10.1016/j.yfrne.2012.08.006. PubMed PMID: 22982535.

11. Kellum JA, Song M, Li J. Science review: extracellular acidosis and the immune response: clinical and physiologic implications. Critical care (London, England). 2004;8(5):331-6. Epub 2004/06/16. doi: 10.1186/cc2900. PubMed PMID: 15469594.

12. Hoogland ICM, Houbolt C, van Westerloo DJ, van Gool WA, van de Beek D. Systemic inflammation and microglial activation: systematic review of animal experiments. Journal of Neuroinflammation. 2015;12(1):114. doi: 10.1186/s12974-015-0332-6.

13. Wiederseiner J-M, Muser J, Lutz T, Hulter HN, Krapf R. Acute Metabolic Acidosis: Characterization and Diagnosis of the Disorder and the Plasma Potassium Response. Journal of the American Society of Nephrology. 2004;15(6):1589. doi: 10.1097/01.ASN.0000125677.06809.37.

14. Singh V, Khatana S, Gupta P. Blood gas analysis for bedside diagnosis. National journal of maxillofacial surgery. 2013;4(2):136-41. doi: 10.4103/0975-5950.127641. PubMed PMID: 24665166.

15. Sood P, Paul G, Puri S. Interpretation of arterial blood gas. Indian journal of critical care medicine : peer-reviewed, official publication of Indian Society of Critical Care Medicine. 2010;14(2):57-64. doi: 10.4103/0972-5229.68215. PubMed PMID: 20859488.

16. de Nadai TR, de Nadai MN, Albuquerque AAS, de Carvalho MTM, Celotto AC, Evora PRB. Metabolic Acidosis Treatment as Part of a Strategy to Curb Inflammation. International Journal of Inflammation. 2013;2013:4. doi: 10.1155/2013/601424.

17. Rehncrona S. Brain acidosis. Annals of Emergency Medicine. 1985;14(8):770-6. doi: https://doi.org/10.1016/S0196-0644(85)80055-X.

18. Wyatt LC, Lewis JS, Andreev OA, Reshetnyak YK, Engelman DM. Applications of pHLIP Technology for Cancer Imaging and Therapy. Trends in Biotechnology. 2017;35(7):653-64. doi: https://doi.org/10.1016/j.tibtech.2017.03.014.

19. Wyatt LC, Moshnikova A, Crawford T, Engelman DM, Andreev OA, Reshetnyak YK. Peptides of pHLIP family for targeted intracellular and extracellular delivery of cargo molecules to tumors. Proceedings of the National Academy of Sciences. 2018;115(12):E2811. doi: 10.1073/pnas.1715350115.

20. Demoin DW, Wyatt LC, Edwards KJ, Abdel-Atti D, Sarparanta M, Pourat J, Longo VA, Carlin SD, Engelman DM, Andreev OA, Reshetnyak YK, Viola-Villegas N, Lewis JS. PET Imaging of Extracellular pH in Tumors with (64)Cu- and (18)F-Labeled pHLIP Peptides: A Structure–Activity Optimization Study. Bioconjugate Chemistry. 2016;27(9):2014-23. doi: 10.1021/acs.bioconjchem.6b00306. PubMed PMID: PMC5034329.

21. Roberts S, Strome A, Choi C, Andreou C, Kossatz S, Brand C, Williams T, Bradbury M, Kircher MF, Reshetnyak YK, Grimm J, Lewis JS, Reiner T. Acid specific dark quencher QC1 pHLIP for multi-spectral optoacoustic diagnoses of breast cancer. Scientific Reports. 2019;9(1):8550. doi: 10.1038/s41598-019-44873-1.

22. John M, Vasso A, Eliada L, George D, Minos-Timotheos M, Maria K, Theodore T, Spyros D. Round and Round we Go: Cyclic Peptides in Disease. Current Medicinal Chemistry. 2006;13(19):2221-32. doi: http://dx.doi.org/10.2174/092986706777935113.

23. Weerakkody D, Moshnikova A, El-Sayed NS, Adochite R-C, Slaybaugh G, Golijanin J, Tiwari RK, Andreev OA, Parang K, Reshetnyak YK. Novel pH-Sensitive Cyclic Peptides. Scientific Reports. 2016;6:31322. doi: 10.1038/srep31322 https://www.nature.com/articles/srep31322#supplementary-information.

24. Varatharaj A, Galea I. The blood-brain barrier in systemic inflammation. Brain, Behavior, and Immunity. 2017;60:1-12. doi: https://doi.org/10.1016/j.bbi.2016.03.010.

25. Gibot S, Buonsanti C, Massin F, Romano M, Kolopp-Sarda M-N, Benigni F, Faure GC, Béné M-C, Panina-Bordignon P, Passini N, Lévy B. Modulation of the triggering receptor expressed on the myeloid cell type 1 pathway in murine septic shock. Infection and immunity. 2006;74(5):2823-30. doi: 10.1128/IAI.74.5.2823-2830.2006. PubMed PMID: 16622220.

26. Allolio C, Magarkar A, Jurkiewicz P, Baxová K, Javanainen M, Mason PE, Šachl R, Cebecauer M, Hof M, Horinek D, Heinz V, Rachel R, Ziegler CM, Schröfel A, Jungwirth P. Arginine-rich cell-penetrating peptides induce membrane multilamellarity and subsequently enter via formation of a fusion pore. Proceedings of the National Academy of Sciences. 2018;115(47):11923-8. doi: 10.1073/pnas.1811520115.

27. Waterhouse RN. Determination of lipophilicity and its use as a predictor of blood–brain barrier penetration of molecular imaging agents. Molecular Imaging & Biology. 2003;5(6):376-89. doi: https://doi.org/10.1016/j.mibio.2003.09.014.

28. Wei L, Easmon J, Nagi RK, Muegge BD, Meyer LA, Lewis JS. 64Cu-Azabicyclo[3.2.2]Nonane Thiosemicarbazone Complexes: Radiopharmaceuticals for PET of Topoisomerase II Expression in Tumors. Journal of Nuclear Medicine. 2006;47(12):2034-41.

29. Chaney AM, Johnson EM, Cropper HC, James ML. PET Imaging of Neuroinflammation Using [11C]DPA-713 in a Mouse Model of Ischemic Stroke. Journal of visualized experiments : JoVE. 2018(136):57243. doi: 10.3791/57243. PubMed PMID: 29985311.

30. James ML, Shen B, Zavaleta CL, Nielsen CH, Mesangeau C, Vuppala PK, Chan C, Avery BA, Fishback JA, Matsumoto RR, Gambhir SS, McCurdy CR, Chin FT. New positron emission tomography (PET) radioligand for imaging σ-1 receptors in living subjects. J Med Chem. 2012;55(19):8272-82. Epub 2012/09/20. doi: 10.1021/jm300371c. PubMed PMID: 22853801.

31. James ML, Belichenko NP, Shuhendler AJ, Hoehne A, Andrews LE, Condon C, Nguyen T-VV, Reiser V, Jones P, Trigg W, Rao J, Gambhir SS, Longo FM. [(18)F]GE-180 PET Detects Reduced Microglia Activation After LM11A-31 Therapy in a Mouse Model of Alzheimer's Disease. Theranostics. 2017;7(6):1422-36. doi: 10.7150/thno.17666. PubMed PMID: PMC5436503.

32. Lively S, Schlichter LC. Microglia Responses to Pro-inflammatory Stimuli (LPS, IFNγ+TNFα) and Reprogramming by Resolving Cytokines (IL-4, IL-10). Frontiers in cellular neuroscience. 2018;12:215-. doi: 10.3389/fncel.2018.00215. PubMed PMID: 30087595.

33. Furube E, Kawai S, Inagaki H, Takagi S, Miyata S. Brain Region-dependent Heterogeneity and Dose-dependent Difference in Transient Microglia Population Increase during Lipopolysaccharide-induced Inflammation. Scientific Reports. 2018;8(1):2203. doi: 10.1038/s41598-018-20643-3.

34. Semmler A, Okulla T, Sastre M, Dumitrescu-Ozimek L, Heneka MT. Systemic inflammation induces apoptosis with variable vulnerability of different brain regions. Journal of Chemical Neuroanatomy. 2005;30(2):144-57. doi: https://doi.org/10.1016/j.jchemneu.2005.07.003.

35. Okuyama S, Makihata N, Yoshimura M, Amakura Y, Yoshida T, Nakajima M, Furukawa Y. Oenothein B suppresses lipopolysaccharide (LPS)-induced inflammation in the mouse brain. International journal of molecular sciences. 2013;14(5):9767-78. doi: 10.3390/ijms14059767. PubMed PMID: 23652834.

36. Skelly DT, Hennessy E, Dansereau MA, Cunningham C. A systematic analysis of the peripheral and CNS effects of systemic LPS, IL-1beta, [corrected] TNF-alpha and IL-6 challenges in C57BL/6 mice. PLoS One. 2013;8. doi: 10.1371/journal.pone.0069123.

37. Bennett ML, Bennett FC, Liddelow SA, Ajami B, Zamanian JL, Fernhoff NB, Mulinyawe SB, Bohlen CJ, Adil A, Tucker A, Weissman IL, Chang EF, Li G, Grant GA, Hayden Gephart MG, Barres BA. New tools for studying microglia in the mouse and human CNS. Proceedings of the National Academy of Sciences. 2016;113(12):E1738-E46. doi: 10.1073/pnas.1525528113.

38. Zhang X, Dong H, Zhang S, Lu S, Sun J, Qian Y. Enhancement of LPS-Induced Microglial Inflammation Response via TLR4 Under High Glucose Conditions. Cellular Physiology and Biochemistry. 2015;35(4):1571-81. doi: 10.1159/000373972.

39. Catorce MN, Gevorkian G. LPS-induced Murine Neuroinflammation Model: Main Features and Suitability for Pre-clinical Assessment of Nutraceuticals. Current Neuropharmacology. 2016;14(2):155-64. doi: 10.2174/1570159X14666151204122017. PubMed PMID: PMC4825946.

40. Narayanaswami V, Dahl K, Bernard-Gauthier V, Josephson L, Cumming P, Vasdev N. Emerging PET Radiotracers and Targets for Imaging of Neuroinflammation in Neurodegenerative Diseases: Outlook Beyond TSPO. Molecular Imaging. 2018;17:1536012118792317. doi: 10.1177/1536012118792317.

41. Chen LQ, Randtke EA, Jones KM, Moon BF, Howison CM, Pagel MD. Evaluations of Tumor Acidosis Within In Vivo Tumor Models Using Parametric Maps Generated with Acido CEST MRI. Molecular imaging and biology : MIB : the official publication of the Academy of Molecular Imaging. 2015;17(4):488-96. doi: 10.1007/s11307-014-0816-2. PubMed PMID: 25622809.

42. Hingorani DV, Randtke EA, Pagel MD. A CatalyCEST MRI Contrast Agent That Detects the Enzyme-Catalyzed Creation of a Covalent Bond. Journal of the American Chemical Society. 2013;135(17):6396-8. doi: 10.1021/ja400254e.

43. Jones KM, Pollard AC, Pagel MD. Clinical applications of chemical exchange saturation transfer (CEST) MRI. Journal of magnetic resonance imaging : JMRI. 2018;47(1):11-27. Epub 2017/08/09. doi: 10.1002/jmri.25838. PubMed PMID: 28792646.

44. Longo DL, Bartoli A, Consolino L, Bardini P, Arena F, Schwaiger M, Aime S. In Vivo Imaging of Tumor Metabolism and Acidosis by Combining PET and MRI-CEST pH Imaging. Cancer Research. 2016;76(22):6463-70. doi: 10.1158/0008-5472.Can-16-0825.

45. Gallagher FA, Kettunen MI, Brindle KM. Imaging pH with hyperpolarized 13C. NMR in Biomedicine. 2011;24(8):1006-15. doi: 10.1002/nbm.1742.

46. Guglielmetti C, Najac C, Didonna A, Van der Linden A, Ronen SM, Chaumeil MM. Hyperpolarized ¹³C MR metabolic imaging can detect neuroinflammation in vivo in a multiple sclerosis murine model. Proceedings of the National Academy of Sciences. 2017;114(33):E6982. doi: 10.1073/pnas.1613345114.

47. Pike VW. PET Radiotracers: crossing the blood-brain barrier and surviving metabolism. Trends in pharmacological sciences. 2009;30(8):431-40. doi: 10.1016/j.tips.2009.05.005. PubMed PMID: PMC2805092.

48. Ortega-Ram, #x00ED, rez A, Vega R, Soto E. Acid-Sensing Ion Channels as Potential Therapeutic Targets in Neurodegeneration and Neuroinflammation. Mediators of Inflammation. 2017;2017:18. doi: 10.1155/2017/3728096.

49. Brown D, Melamed ML. New Frontiers in Treating Uremic Metabolic Acidosis. Clinical Journal of the American Society of Nephrology. 2018;13(1):4-5. doi: 10.2215/cjn.11771017.

50. Kraut JA, Raphael KL. Drug removal of gastric acid: a novel treatment of metabolic acidosis. The Lancet. 2019;394(10196):363-4. doi: 10.1016/S0140-6736(19)31473-4.

51. Zhou R-P, Wu X-S, Wang Z-S, Xie Y-Y, Ge J-F, Chen F-H. Novel Insights into Acid-Sensing Ion Channels: Implications for Degenerative Diseases. Aging Dis. 2015;7(4):491-501. doi: 10.14336/AD.2015.1213. PubMed PMID: 27493834.

52. Sluka KA, Winter OC, Wemmie JA. Acid-sensing ion channels: A new target for pain and CNS diseases. Curr Opin Drug Discov Devel. 2009;12(5):693-704. PubMed PMID: 19736627.

53. Scheiner B, Lindner G, Reiberger T, Schneeweiss B, Trauner M, Zauner C, Funk G-C. Acid-base disorders in liver disease. Journal of Hepatology. 2017;67(5):1062-73. doi: https://doi.org/10.1016/j.jhep.2017.06.023.